PNAS RESEARCH ARTICLE | PLANT BIOLOGY

Plant ESCRT protein ALIX coordinates with retromer complex in regulating receptor-mediated sorting of soluble vacuolar proteins

Shuai Hu[a], Baiying Li[b], Fan Wu[a], Dongmei Zhu[a], Jan Zouhar[c,d], Caiji Gao[e], Tomoo Shimada[f], Enrique Rojo[d], Ikuko Hara-Nishimura[g], Liwen Jiang[b,h], and Jinbo Shen[a,1]

Edited by Natasha Raikhel, Center for Plant Cell Biology, Riverside, CA; received January 11, 2022; accepted April 12, 2022

Vacuolar proteins play essential roles in plant physiology and development, but the factors and the machinery regulating their vesicle trafficking through the endomembrane compartments remain largely unknown. We and others have recently identified an evolutionarily conserved plant endosomal sorting complex required for transport (ESCRT)-associated protein apoptosis-linked gene-2 interacting protein X (ALIX), which plays canonical functions in the biogenesis of the multivesicular body/prevacuolar compartment (MVB/PVC) and in the sorting of ubiquitinated membrane proteins. In this study, we elucidate the roles and underlying mechanism of ALIX in regulating vacuolar transport of soluble proteins, beyond its conventional ESCRT function in eukaryotic cells. We show that ALIX colocalizes and physically interacts with the retromer core subunits Vps26 and Vps29 in planta. Moreover, double-mutant analysis reveals the genetic interaction of *ALIX* with *Vps26* and *Vps29* for regulating trafficking of soluble vacuolar proteins. Interestingly, depletion of ALIX perturbs membrane recruitment of Vps26 and Vps29 and alters the endosomal localization of vacuolar sorting receptors (VSRs). Taken together, ALIX functions as a unique retromer core subcomplex regulator by orchestrating receptor-mediated vacuolar sorting of soluble proteins.

vacuolar trafficking | endosomal recycling | multivesicular body/prevacuolar compartment (MVB/PVC) | ESCRT machiner | retromer complex

Significance

The endosomal sorting complex required for transport (ESCRT) machinery in multicellular organisms plays canonical functions in multivesicular body (MVB) biogenesis and membrane protein sorting. Nonetheless, its critical role in the sorting of soluble vacuolar proteins and its interplay with endosomal recycling machinery have yet to be reported. In this study, we demonstrate that *Arabidopsis* ESCRT-associated ALIXinteracts with the retromer core subunitsto regulate their recruitment onto endosome membrane for recycling of vacuolar sorting receptors (VSRs) for efficient sorting of soluble vacuolar proteins. This work provides molecular insights into the unique properties of ALIX in regulating vacuolar transport of soluble proteins, thus shedding new light on the crosstalk and coordination between the vacuolar trafficking and endosomal recycling pathways in plants.

Membrane trafficking in the plant endomembrane system is critical for multiple processes in plant growth and development as well as survival under various stress conditions (1, 2). Although the endomembrane system is mostly conserved among eukaryotes, intracellular trafficking in plant cells has its own unique properties and functions. One feature especially stands out prominently: the presence of two types of vacuoles, lytic vacuoles (LVs) and protein storage vacuoles (PSVs) (3). In plants, the selective sorting of hydrolytic enzymes into LVs and storage proteins into PSVs can be mediated by the family of vacuolar sorting receptors (VSRs) (4–6). In this sorting process, newly synthesized soluble proteins—including the major *Arabidopsis* storage proteins 12S globulins and 2S albumins as well as the vacuolar thiol protease aleurain—are synthesized and translocated into the endoplasmic reticulum lumen for subsequent transport into Golgi apparatus followed by the *trans*-Golgi network (TGN). The soluble proteins with vacuolar sorting signals can be recognized by VSRs as cargo and are ultimately deposited into the vacuole via the prevacuolar compartments (PVCs)—also called multivesicular bodies (MVBs)—whereas the proteins without vacuolar sorting signals will be secreted to extracellular space (ECS) (7, 8). Although it is clear that VSRs are essential factors for the correct trafficking of soluble vacuolar proteins, there are many questions remaining about their functioning. For instance, it is still unsettled in which compartments VSRs bind and release their cargoes (9) and how they are then recycled back for additional rounds of cargo sorting (10, 11).

Vacuolar degradation of membrane proteins is important for maintaining homeostasis by recycling nonfunctional or misfolded proteins and also to ensure proper cell signaling and interactions with the environment (12). Key to this process are the formation of intraluminal vesicles (ILVs) and the sorting of ubiquitinated membrane cargoes into ILVs of MVB/PVCs, which is mediated by an evolutionarily conserved machinery called endosomal sorting complex required for transport (ESCRT). The ESCRT machinery comprises a cascade of five multiprotein complexes: ESCRTs (ESCRT-0, -I, -II, and III) and Vps4 complex. Besides the putative homologs for most canonical ESCRT components (13, 14), plants have evolved unique ESCRT components, such as PROS (a positive regulator of SKD1), FYVE (Fab-1, YGL023, Vps27, and EEA1) domain-containing proteins FREE1 (also termed FYVE1) and FYVE4, and putative plant-specific negative regulators that coordinate with ESCRT subunits at MVB/PVCs to sort ubiquitinated protein to LVs (15–20).

Author contributions: S.H., E.R., and J.S. designed research; S.H., B.L., F.W., D.Z., J.Z., T.S., and J.S. performed research; S.H., C.G., E.R., I.H.-N., and J.S. analyzed data; and E.R., L.J., and J.S. wrote the paper.

The authors declare no competing interest.

This article is a PNAS Direct Submission.

Copyright © 2022 the Author(s). Published by PNAS. This article is distributed under Creative Commons Attribution-NonCommercial-NoDerivatives License 4.0 (CC BY-NC-ND).

[1]To whom correspondence may be addressed. Email: jshen@zafu.edu.cn.

This article contains supporting information online at http://www.pnas.org/lookup/suppl/doi:10.1073/pnas.2200492119/-/DCSupplemental.

Published May 9, 2022.

Arabidopsis ALIX (also termed AtBRO1), a homolog of human apoptosis-linked gene-2 interacting protein X (ALIX) and budding yeast bypass of C kinase 1 (BCK1)-like resistance to osmotic shock 1p (Bro1p), is an ESCRT-associated protein that aids the function of ESCRT complexes at the MVB/PVCs. *Arabidopsis* ALIX interacts with the ESCRT-III via the charged MVB protein 4/sucrose nonfermenting 7 (CHMP4/Snf7) subunit that facilitates cargo sorting and ILV formation and recruits the deubiquitinating enzyme AMSH to MVB/PVCs to remove ubiquitins from ubiquitinated membrane cargoes before internalization of the cargoes into ILVs (21, 22). Although ALIX has been assumed to function in the degradation of membrane cargo proteins, such as the phosphate transporters PHT1 and auxin efflux carrier PIN1 (22, 23), it has also been suggested that ALIX may coordinate vacuolar degradation of the membrane-associated abscisic acid receptor (24). Interestingly, our recent studies have also demonstrated that the mutants of ALIX display defects in embryogenesis and seed germination (23); thus, it is possible that ALIX regulates additional processes, possibly by mediating trafficking of other protein cargoes.

In this study, we identify another branch of ALIX function that regulates transport of plant soluble vacuolar proteins. We first identified the retromer core subunits Vps26 and Vps29 as unique direct interactors. Through a combination of cellular, biochemical, and genetic approaches, we further present evidence for a unique role for ALIX in the recruitment of Vps26 and Vps29 to endosomal membranes, thereby functioning as an important regulator in orchestrating VSR-mediated soluble vacuolar proteins transport.

Results

ALIX Is Required for the Soluble Vacuolar Protein Transport. Recent studies have identified a plant ALIX, which functions as an ESCRT-associated protein in controlling the formation of ILVs in MVB/PVCs and regulating transport of membrane proteins to vacuoles (21–24). ALIX is essential for plant embryogenesis, and its depletion causes seedling lethality (21–23). To investigate the potential roles of ALIX in regulating MVB/PVC-mediated transport of seed storage proteins to PSVs or hydrolases to LVs in seedlings, we here studied four different genotypes affected in ALIX function (*SI Appendix*, Fig. S1*A*): two transfer DNA (T-DNA) insertional mutants, *alix-2* (also named *atbro1-1*) and *alix-4*, which show defects in plant embryogenesis; the hypomorphic *alix-1* mutant, which contains a mis-sense glycine^{260}-to-aspartic acid (G260D) mutation in the BRO1 domain of ALIX; and a dexamethasone (DEX)-inducible *RNAi* line (*DEX::ALIX-RNAi*), which shows seedling growth defects after DEX-induced *ALIX* silencing (*SI Appendix*, Fig. S1*B*) (21–23). Around a quarter of paler seeds in *alix-2* or *alix-4* (21.78% in *alix-2*, $n = 377$; 21.2% in *alix-4*, $n = 423$) were observed in the siliques from self-pollinated heterozygous mutants, which were identified as homozygous mutants by genotyping and a complementation study using *ALIXpro::GFP-ALIX* (Fig. 1*A* and *SI Appendix*, Fig. S1*C*). The *alix-2*$^{(+/-)}$ or *alix-4*$^{(+/-)}$ mutants were then crossed with the plant PSV cargo marker green fluorescent protein (GFP)-CT24 (5). Interestingly, GFP fluorescence signals were observed under ultraviolet (UV) light in large numbers of developing or mature seeds from the self-pollinated *alix-2*$^{(+/-)}$ and *alix-4*$^{(+/-)}$ mutants. Instead, the seeds of wild-type (WT) expressing GFP-CT24, in which GFP was stored in PSVs, displayed only low background signals (Fig. 1*B* and *SI Appendix*, Fig. S1*D*). Genotyping confirmed that the green seeds under UV were homozygous mutants.

The green fluorescent seeds might be defective in GFP-CT24 vacuolar trafficking (5). To determine the localization of GFP-CT24 in *alix* mutants, mature seeds were dissected and subjected to confocal laser scanning microscope observation. In WT or heterozygous embryos, signals of GFP-CT24 overlapped with the autofluorescence of the PSV, whereas in mature seeds of *alix-2* or *alix-4*, GFP-CT24 was predominantly secreted into the ECSs (Fig. 1*C*). In addition, the secretion of GFP-CT24 was observed in developing embryo cells of both *alix-2* and *alix-4* mutants (*SI Appendix*, Fig. S1*E*). To further verify the defects of PSV transport of storage proteins in the *alix* mutants, the homozygous *alix-2* or *alix-4* seeds identified by their green signals were collected to analyze the protein profile of endogenous seed storage proteins, and two major seed storage proteins, 2S albumin and 12S globulin, were chosen as markers. As shown in Fig. 1*D*, precursor proteins of both 2S albumin (p2S) and 12S globulin (p12S) accumulated in both *alix-2* and *alix-4* mutants as indicated by Coomassie blue staining and immunoblots with anti-2S albumin and anti-12S globulin antibodies in total protein extracts from seeds. In addition, compared to the WT seeds, higher amounts of GFP-CT24 were also accumulated in both *alix-2* and *alix-4* mutants (Fig. 1*D*), which is probably due to the increased stability of GFP-CT24 in the ECSs of seed cells (5).

To gain further insight into the effects of the *alix* mutation at the ultrastructural level, we next performed transmission electron microscopic (TEM) analysis in combination with immunogold labeling in ultrathin sections of embryos prepared by high-pressure frozen/freeze-substituted fixation (HPF/FS). Electron micrographs revealed that the ECS of the *alix-2* embryo cells filled with electron-dense material compared to WT seeds (Fig. 1 *E* and *F*). Immunogold analysis with 12S globulin (Fig. 1*E*) and 2S albumin (Fig. 1*F*) demonstrated that abundant gold particles were presented in ECS of *alix-2* embryo cells, while gold particles were found exclusively in PSVs of WT embryos. Intriguingly, a large number of 12S globulin- and 2S albumin-positive and electron-dense structures accumulated in the ECS of *alix-2* embryo cells (Fig. 1 *G* and *H*), which may be released after fusion of the storage proteins containing vesicle membrane with the plasma membrane (PM) of the cell.

In addition, loss of ALIX impairs transport of soluble vacuolar proteins to LVs. We observed that the LV cargo marker RFP fusion with vacuolar sorting signal (spL-RFP) (25) was predominantly secreted into the ECSs in root cells of *DEX::ALIX-RNAi* seedlings after DEX induction (Fig. 1*I*). Similarly, the secretion of spL-RFP into the ECSs can also be observed in the *alix-1* mutant (Fig. 1*J*). To further confirm the function of ALIX in vacuolar trafficking of soluble cargo, we crossed the synthetic vacuolar cargo VAC2 transgene plant into the *alix-1* mutant (26). In WT plants, VAC2 localizes to the LVs, where it is inactive and has no effect on plant growth and development (26). However, interference with vacuolar trafficking may lead to VAC2 secretion. In the apoplast, VAC2 inhibits the WUSCHEL signaling pathway, reducing the size of the shoot apical meristem (SAM) and even leading to SAM termination if secretion is strong (27, 28). In the F2 population, we observed that *alix-1* homozygous mutants with the VAC2 transgene had terminated SAMs, whereas all the controls, including homozygous *alix-1* plants without the VAC2 transgene and heterozygous *alix-1* plants with the VAC2 transgene, had normal indeterminate meristems (Fig. 1*K* and *SI Appendix*, Fig. S1*F*). These data provide an additional confirmation of the role of ALIX in trafficking soluble vacuolar cargoes into LVs.

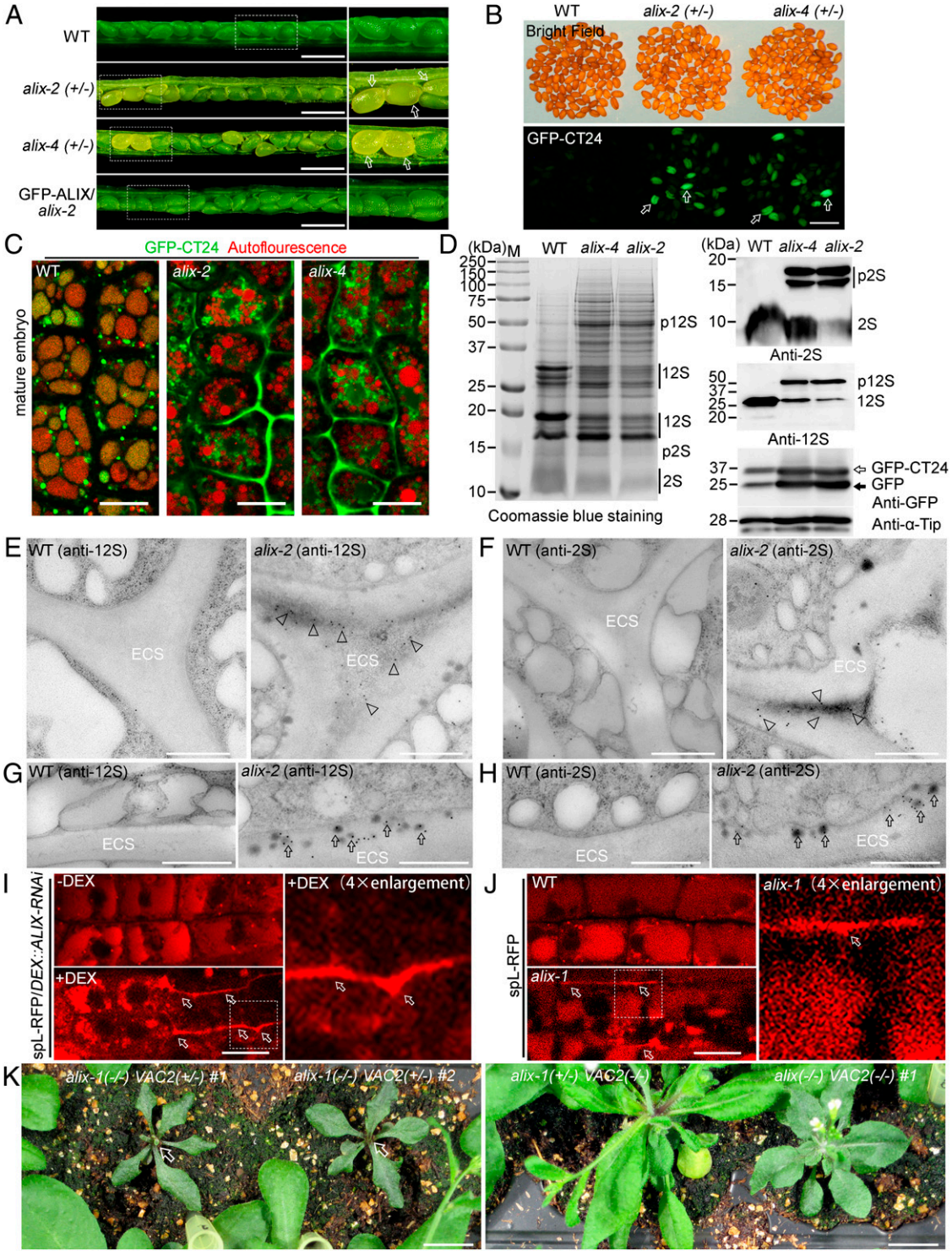

Fig. 1. ALIX regulates the transport of vacuolar proteins to both PSVs and LVs. (*A*) ALIX is essential for plant seeds' development. Siliques from WT, *alix-2* and *alix-4* heterozygous mutant plants, and complementation plant of *alix-2* with *GFP-ALIX*. Note the paler seeds in the *alix* heterozygous mutant plant siliques (arrow). Scale bar, 1 mm. (*B*) The *alix* mutants that express GFP-CT24 produce green fluorescent seeds. GFP-CT24 was expressed in the WT, *alix-2*$^{(+/-)}$, and *alix-4*$^{(+/-)}$ heterozygous plants. The seeds of the F2 population were inspected with a binocular microscope (*Top*) or an epifluorescent microscope (*Bottom*). Both GFP-CT24/*alix-2*$^{(+/-)}$ and GFP-CT24/*alix-4*$^{(+/-)}$ produced green fluorescent seeds (arrows). Scale bar, 1 mm. (*C*) GFP-CT24 in mature embryo cells of the WT and *alix* mutant. The GFP-CT24 (green) overlaps with the autofluorescence of the seed storage vacuoles (red) in WT, whereas it is secreted to the ECSs in both *alix-2 and alix-4* mutant cells. Scale bars, 10 μm. (*D*) The *alix* mutant is defective in processing of seed storage proteins. The WT seeds and the selected green fluorescent seeds in the GFP-CT24/*alix-2*$^{(+/-)}$ and GFP-CT24/*alix-4*$^{(+/-)}$ mutant plant were subjected to protein extraction for Coomassie blue staining (*Left*) or immunoblot analysis (*Right*) with anti-12S globulin, anti-2S albumin, or anti-GFP antibodies. Note the accumulation of precursors of storage proteins in *alix* mutant seeds. Anti-α-Tip, a tonoplast intrinsic protein, is used as a loading control. (*E* and *F*) Immunoelectron micrograph of WT and *alix-2* embryo cells with anti-12S globulin (*E*) or anti-2S albumin (*F*). Storage proteins were secreted into the electron-dense ECS in the *alix* mutant embryo cells (arrowheads). Scale bars, 500 nm. (*G* and *H*) Enlarged image of an immunoelectron micrograph of WT and *alix-2* mutant embryo cells with anti-12S globulin (*G*) or anti-2S albumin (*H*) antibody, showing the distribution of the electron-dense structures (arrows) in the ECS of *alix-2* mutant. Scale bars, 500 nm. (*I* and *J*) Confocal microscopic images of the soluble LV cargo spL-RFP expressed in *DEX::ALIX-RNAi* plant in the absence (–) or presence (+) of DEX (*I*) as well as *alix-1* mutant (*J*). Note the secretion of spL-RFP to the ECS (arrows). The regions within the white outline are enlarged (*Right*) (magnification: 4×). Scale bars, 10 μm. (*K*) Phenotypes of the F2 population of *alix-1*$^{(+/-)}$ *VAC2*$^{(+/-)}$. Note only the *alix-1*$^{(-/-)}$ *VAC2*$^{(+/-)}$ had phenotype of terminated SAMs (arrows). Scale bars, 1 cm.

Taken together, these results suggest that ALIX plays a crucial role in transport of soluble vacuolar proteins into both PSVs and LVs.

ALIX Is Incorporated into the Retromer Complex via a Direct Interaction with Vps26 and Vps29. To explore the possible molecular mechanism of ALIX function in soluble vacuolar protein sorting, we first searched for potential interactor(s). To this aim, we performed coimmunoprecipitation (co-IP) experiments with protein extracts of GFP or GFP-ALIX plants using anti-GFP antibodies followed by liquid chromatography–tandem mass spectrometry (LC-MS/MS) analysis (*SI Appendix*, Fig. S2*A*). Identified proteins included Vps26A and Vps35A, which are core subunits of the retromer complex (Fig. 2*A*). The retromer complex, conserved across eukaryotes, contains the core subunits (Vps26, Vps29, and Vps35) and associated sorting nexin (SNX) dimers (29–31). To explore the possible molecular links between ALIX and the retromer complex, we next cloned other subunits of plant retromer complexes for yeast two-hybrid (Y2H) binary assays and found that ALIX interacted with both *Arabidopsis* Vps26 homologs (Vps26A and Vps26B) and Vps29, but not with Vps35 homologs or SNXs (Fig. 2*B* and *SI Appendix*, Fig. S2*B*). Because *Arabidopsis* ALIX also associates with the ESCRT-III components (21, 22), we tested whether other ESCRT-III components form a protein complex with retromer. Interestingly, we did not observe any interaction of Vps26 homologs or Vps29 with each of ESCRT-III components (Vps2.1, Vps24, Vps20A, SNF7A, and SNF7B), FREE1/FYVE1 (17, 18), FYVE4 (16), and de-ubiquitinating enzyme AMSH1 in the Y2H binary assays (*SI Appendix*, Fig. S2*C*). All these data point to the specific interaction of ALIX with retromer core subunits Vps26 and Vps29.

The interaction of ALIX with Vps26 homologs or Vps29 was further confirmed in planta by IP between Myc-tagged ALIX and enhanced yellow fluorescent protein (EYFP)-tagged Vps26A, Vps26B, or Vps29 with negative control Vps28A (*SI Appendix*, Fig. S2*D*). When performing acceptor photobleaching-fluorescence resonance energy transfer (FRET-AB) analysis, EYFP-Vps26A, EYFP-Vps26B, and EYFP-Vps29, but not EYFP-Vps28A, showed strong interactions with Cerulean-ALIX in punctate compartments of protoplasts isolated from *Arabidopsis*plant system biology dark-type culture (PSB-D) cells (Fig. 2*C*). In addition, an IP assay using protein extracts from *Arabidopsis* cells coexpressing hemagglutinin (HA)-tagged Vps26A, Myc-tagged Vps29, Vps35A, and EYFP-tagged ALIX showed that 3×HA-Vps26A, Vps29-5×Myc, and Vps35A-5×Myc were IP by EYFP-ALIX, but not by the EYFP control (Fig. 2*D*), thus supporting the association of whole retromer core subunits with ALIX in the same protein complex.

ALIX protein consists of an N-terminal BRO1 domain (BRO1D) followed by a V-ALIX domain (ALIXD) and a C-terminal proline-rich region (PRR) (Fig. 2*E*). To clarify the domain(s) in ALIX required for interaction with Vps26 or Vps29, we generated different ALIX fragments for Y2H interaction analysis. As shown in Fig. 2*E*, the ALIXD and the C-terminal PRR region were dispensable for the interaction with Vps26 homologs or Vps29, whereas the BRO1D domain was sufficient for the interaction. Similar results also showed that deletion of the BRO1 domain of ALIX (ALIX-Δ*bro1d*) abolished its interaction with the Vps26 homologs or Vps29 (Fig. 2*E*). Interestingly, ALIX(G260D), a mis-sense mutation in the BRO1 domain of ALIX in the *alix-1* line, abolished the interaction with Vps29 and displayed reduced interaction with Vps26A or Vps26B compared to the WT version (Fig. 2 *F* and *G*). To further confirm the domain(s) in ALIX that directly interact with Vps26 and Vps29, we purified recombinant His-Small Ubiquitin-like Modifier (SUMO)-tagged BRO1D, ALIXD, and PRR region together with glutathione S-transferase (GST), GST-Vps26A, and GST-Vps29 (*SI Appendix*, Fig. S2*E*). In these *in vitro* binding assays, we found that the N-terminal BRO1D, but neither ALIXD nor PRR region of ALIX, can directly interact with Vps26A or Vps29 (*SI Appendix*, Fig. S2*F*). Taken together, we demonstrated that ALIX was incorporated into the retromer core complex via a direct interaction with Vps26 and Vps29 through the N-terminal BRO1D, and the mutation in *alix-1* decreased the interaction ability.

ALIX Colocalizes with Both Vps26 and Vps29 on MVB/PVCs in Embryo and Root Cells. If ALIX functions together with Vps26 and Vps29, they should show overlapping subcellular localizations. Although the functions of retromer subunits in regulating soluble cargo vacuolar transport have been well documented, their subcellular localization in plants is still controversial (11, 32). The differences in subcellular localization may be due to the different association of the retromer complex with distinct membrane populations in different materials or during different plant growth stages (33). In particular, the subcellular distribution of Vps26 has not been investigated. Thus, we further explored the subcellular localization of Vps26 and Vps29 with ALIX in both embryos and root epidermal cells.

To this aim, we expressed *Vps26Apro::Vps26A-GFP* and *Vps29pro::Vps29-GFP* constructs in plants and crossed with different endosomal markers to examine their localization in embryo cells. The Vps26A-GFP punctae mainly colocalized with the MVB/PVC marker mCherry-Rha1 (69.5 ± 8.2%, n = 1462) but did not show efficient colocalization with the TGN/early endosome (EE) marker VHA-a1-RFP (17.3 ± 2.7%, n = 992) or Golgi marker mCherry-SYP32 (12.7 ± 4.2%, n = 869) (Fig. 3 *A* and *B*). Similarly, Vps29-GFP punctae also showed high frequent colocalization with mCherry-Rha1 vesicles (67.4 ± 6.5%, n = 975), partially colocalized with the TGN/EE marker (24.2 ± 3.9%, n = 913), but separated from the Golgi marker (16.3 ± 5.0%, n = 989) (*SI Appendix*, Fig. S3). Thus, these data indicate that the Vps26A-GFP and Vps29-GFP punctae represent mainly MVB/PVCs. To further establish the MVB/PVC localization of Vps26A and Vps29, we treated the Vps26A-GFP/mCherry-Rha1 or Vps29-GFP/mCherry-Rha1 coexpressing line with the PI3K/PI4K inhibitor wortmannin (Wort), which induces MVB/PVC homotypic fusion and results in enlarged MVB/PVCs (34). Indeed, in Wort-treated cells, Vps26A-GFP or Vps29-GFP and mCherry-Rha1 showed colocalization to the surface of the enlarged MVB/PVCs that appeared as ring-like structures (Fig. 3*C*). The MVB/PVCs localization of Vps26A and Vps29 have also been confirmed in root epidermal cells (*SI Appendix*, Fig. S4). Collectively, these results demonstrate that Vps26 and Vps29 mainly localize on MVB/PVCs in the *Arabidopsis* plant.

In *Arabidopsis*, ALIX has been indicated to be distributed in cytosol and partially localized on MVB/PVCs in root epidermal cells (21–23). Similarly, in embryo cells, GFP-ALIX signals showed cytosolic distribution but were also localized as intracellular punctate dots with 46.3 ± 8.7% (n = 446) colocalization with the MVB/PVCs marker mCherry-Rha1 and 22.6 ± 4.3% (n = 497) colocalization with the TGN marker VHA-a1-RFP (*SI Appendix*, Fig. S5*A*). When transiently expressed in protoplasts of *Arabidopsis* suspension cells, 48.2 ± 3.9% GFP-ALIX punctae (n = 244) colocalized with the MVB/PVCs marker mRFP-AtVSR2 (*SI Appendix*, Fig. S5*B*). Moreover, in root epidermal cells, GFP-ALIX punctae showed 38.7 ± 4.6% (n = 2,040) colocalization with endogenous VSRs (Fig. 3*D*).

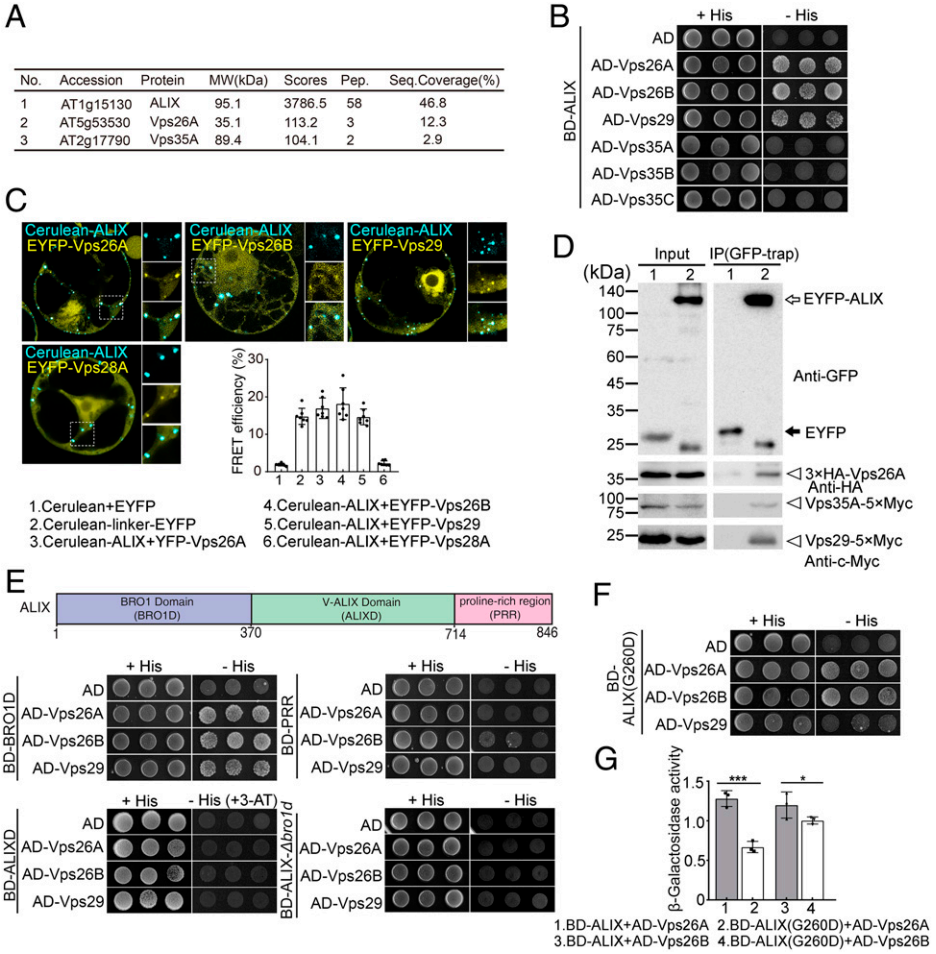

Fig. 2. ALIX interacts directly with retromer subunits Vps26 and Vps29. (*A*) Proteins identified by tandem mass spectrometry after IP of GFP-ALIX. Five-day-old transgenic *Arabidopsis* seedlings expressing GFP or GFP-ALIX were subjected to GFP-trap following by LC-MS/MS analysis to identify potential interactors. Vps26A (No.2) and Vps35A (No.3) were identified as interacting partner of ALIX. Pep., the number of peptides identified in MS; Seq. coverage, the percentage of the protein sequence covered by identified peptides. (*B*) Y2H analysis of the binary interactions of ALIX with retromer core subunits Vps26A/B, Vps29, and Vps35A/B/C. Transformed yeast cells were grown on plates containing either synthetic complete medium lacking leucine and tryptophan (with histidine, +His) as a transformation control or synthetic complete medium lacking histidine as well as leucine and tryptophan (without histidine, −His) for interaction assays. (*C*) FRET analysis of the colocalized punctae between Cerulean-ALIX and the two Vps26 homologs (EYFP-Vps26A and EYFP-Vps26B), EYFP-Vps29, or control EYFP-Vps28A. FRET efficiency was quantified by using the AB approach (*Right*, *Bottom*). For each group, seven individual protoplasts were used for FRET efficiency quantification and statistical analysis. Error bars are the SD of FRET efficiency. Scale bars, 10 μm. (*D*) IP assay shows association among Vps26A, Vps29, and Vps35A with ALIX. *Arabidopsis* protoplasts expressing EYFP (lane 1) or EYFP-ALIX (lane 2) with 3×HA-Vps26A, Vps29-5×Myc, and Vps35A-5×Myc were subjected to protein extraction and IP with GFP-trap followed by immunoblot with indicated antibodies. Arrowhead indicates Vps26A, Vps29, and Vps35A proteins co-IP by ALIX. (*E*) Y2H analysis of the binary interactions between Vps26A, Vps26B, or Vps29 and different deletions or mutation forms of ALIX. 3-AT is used to suppress the background self-activation of the BD genes. (*F*) Y2H analysis of the binary interactions between Vps26A, Vps26B, or Vps29 and ALIX(G260D). (*G*) Quantification analysis of interaction ability of ALIX or ALIX(G260D) with Vps26A and Vps26B in Y2H analysis. β-galactosidase assays were performed on yeast cotransfected with plasmids expressing indicated recombinant proteins. Error bars represent the SD from three independent assays. $*P < 0.05$, $***P < 0.001$ in Student's *t* test.

Therefore, consistent with previous reports, ALIX partially localizes to MVB/PVCs. If ALIX localizes to MVB/PVCs, it should show overlapping intracellular localizations with Vps26 and Vps29. Indeed, Vps26A-mCherry or Vps29-mCherry colocalized with GFP-ALIX in intracellular punctate dots in both embryo cells (27.4 ± 9.8%, $n = 339$; 38.9 ± 6.7%, $n = 330$) (Fig. 3*E*) and root epidermal cells (13.9 ± 1.1%, $n = 345$; 17.2 ± 2.8%, $n = 332$) (*SI Appendix*, Fig. S5*C*). In Wort-treated cells, GFP-ALIX colocalized with Vps26A-mCherry or Vps29-mCherry on swollen MVBs (Fig. 3*F*). Taken together, these results demonstrate that ALIX colocalizes with Vps26 or Vps29 on MVB/PVCs.

Genetic Interactions between ALIX and Vps26 or Vps29 in Soluble Vacuolar Protein Sorting. The interaction and colocalization of ALIX with Vps26 or Vps29 motivated us to determine their possible genetic interactions. The two retromer proteins Vps26 and Vps29 are required in many aspects of plant development, including gametophyte or embryo development as well as seedling survival (29, 35, 36). To this end, we first established *vps26a-1 vps26b-1* and *vps29* mutants. Consistent with previous reports, both *vps26a-1 vps26b-1* double-null mutant and *vps29-3* mutant plants had a dwarf phenotype compared with WT controls (*SI Appendix*, Fig. S6*A*). In addition, *Vps26A-GFP* and *Vps29-GFP*, expressed under control of the native promoters, can complement the respective mutant phenotypes, thus confirming the association of the phenotypes with the respective mutants and suggesting the chimeric proteins are functional in plants. The mutants *vps26a-1*, *vps26b-1*, and *vps29-3* were then crossed with heterozygous *alix-2*$^{(+/-)}$ or the weak allele *alix-1*. Using PCR-based genotyping combined with phenotype observation, we isolated *alix-1 vps26a-1* and *alix-1 vps26b-1* double mutants. However, in an F3 population derived from the self-pollination of *alix-1 vps26a-1 vps26b*$^{(+/-)}$ or *alix-1 vps29-3*$^{(+/-)}$ plant, we were unable to identify viable homozygous *alix-1 vps26a-1 vps26b* triple mutant or *alix-1*

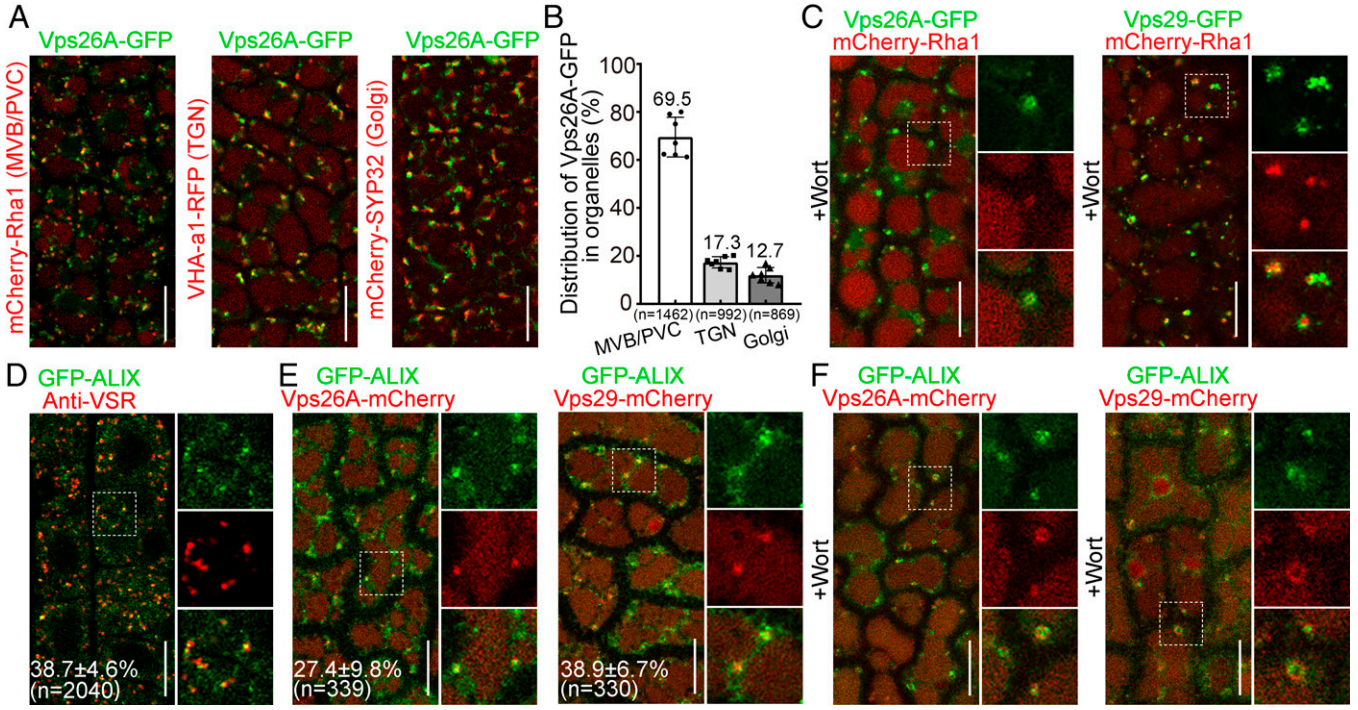

Fig. 3. ALIX colocalizes with Vps26 and Vps29 on MVB/PVCs in plants. (*A*) Colocalization analysis of Vps26A with endosomal markers. Colocalization of Vps26A-GFP with the MVB/PVC marker mCherry-Rha1 (*Left*), TGN/EE marker VHA-a1-RFP (*Center*), and the Golgi marker mCherry-SYP32 (*Right*) were analyzed with a confocal microscope in *Arabidopsis* developing embryo cells. Scale bars, 10 μm. (*B*) Percentage of Vps26A-GFP-positive punctae that colocalize with endosomal markers shown in *A*. The results were obtained from seven individual seedlings. Error bars represent the SD of percentages. n, total numbers of analyzed Vps26A-GFP punctae. (*C*) Colocalization analysis of Vps26A-GFP (*Left*) or Vps29-GFP (*Right*) with MVB/PVC/LE marker mCherry-Rha1 after Wortmannin treatment (+Wort) in embryo cells. Separated images of each channel in the white outlined area are shown on the right side (from top to bottom: GFP, RFP, and merged). Scale bars, 10 μm. (*D*) Colocalization analysis of GFP-ALIX with endogenous VSRs. Immunofluorescent labeling with the MVB/PVC marker anti-VSR antibody in root cells expressing GFP-ALIX. Colocalization was quantified from 10 individual labeling roots. The percentage of anti-VSR-labeled MVB/PVCs with GFP-ALIX vesicle colocalization is included in the bottom. n, total numbers of analyzed GFP-ALIX punctae. Scale bar, 10 μm. (*E*) Colocalization of GFP-ALIX with Vps26A-mCherry (*Left*) or Vps29-mCherry (*Right*). The localization of GFP-ALIX, Vps26A-mCherry, and Vps29-mCherry in developing embryo cells was analyzed under a confocal microscope. The percentage of GFP-ALIX with Vps26A-mCherry or Vps29-mCherry colocalization is included in the bottom. The results were obtained from eight individual embryos. n, total numbers of analyzed GFP-ALIX punctae. Scale bars, 10 μm. (*F*) GFP-ALIX and Vps26A-mCherry (*Left*) or Vps29-mCherry (*Right*) colocalize to wortmannin (+Wort)-induced enlarged MVB/PVCs. Seedlings expressing GFP-ALIX and Vps26A-mCherry or Vps29-mCherry as shown in *E* were treated with Wort for 2 h before imaging. Scale bars, 10 μm.

vps29-3 double mutant, suggesting that the loss of function of these two genes is either gametophytic or embryonic lethal. Indeed, 27.3% ($n = 249$) undeveloped ovules appeared in self-fertilized siliques of 8-wk-old *alix-1 vps29-3*$^{(+/-)}$ mutant (Fig. 4*A*). In addition, we isolated the *alix-2*$^{(+/-)}$ *vps29-3*$^{(+/-)}$ heterozygous and observed about 17.9% ($n = 352$) undeveloped ovules and 23.31% ($n = 352$) aborted embryos in the siliques after their self-fertilization (Fig. 4*A*). These results indicate a synthetic lethal interaction between ALIX and Vps26 or Vps29 mutations on gametophyte and embryo development.

Next, we investigated a possible genetic interaction in regulating seedling growth. When germinated on 1/2 MS agar for 7 d, the root length of *alix-1 vps26a-1*, *alix-1 vps26b-1*, and *alix-1 vps29-3*$^{(+/-)}$ was slightly shorter ($P < 0.05$) compared to their corresponding single mutants or WT plant (Fig. 4*B*). Moreover, the rosette growth rate was also decreased in the double mutants relative to the single mutants and WT plants (*SI Appendix*, Fig. S6*B*), suggesting the ALIX and associated retromer complex play critical roles in the growth of both aerial and belowground organs. Taken together, these data reveal a genetic interaction of ALIX with Vps26 or Vps29 in regulating plant growth.

The maturation of the major seed storage proteins has previously been shown to be altered in Vps26 or Vps29 mutants (35, 36). We next investigated the functional connection among ALIX, Vps26, and Vps29 by exploring the trafficking of vacuolar protein cargo in seeds and young seedlings. We first extracted proteins from the seeds of progenies derived from the self-pollinated *alix-1 vps29-3*$^{(+/-)}$ and *alix-2*$^{(+/-)}$ *vps29-3*$^{(+/-)}$ heterozygous mutant plants and compared to their individual mutants. The proteins were then applied for immunoblot analysis using specific anti-12S globulin antibody. We found the accumulation of p12S in seeds of self-pollinated progenies from *alix-2*$^{(+/-)}$ or *vps29-3*$^{(+/-)}$ plants, but not in seeds from WT or *alix-1* mutant plants (Fig. 4*C*). Consistently, the degree of the p12S accumulation in seeds of progenies from heterozygous *alix-2*$^{(+/-)}$ plants was lower than in samples obtained from homozygous *alix-2* or *alix-4* seeds (Fig. 1*D*). In addition, seeds of progenies from *alix-2*$^{(+/-)}$ *vps29-3*$^{(+/-)}$ plants showed higher ($P < 0.05$) accumulation of p12S than those from WT, *alix-2*$^{(+/-)}$, or *vps29-3*$^{(+/-)}$ plants (Fig. 4*D*). Interestingly, in contrast to the presence of p12S proteins in seeds from *vps29-3*$^{(+/-)}$ plants, no accumulation of p12S is detected in seeds of self-pollinated progenies from *alix-1 vps29-3*$^{(+/-)}$ plants, most likely reflecting the absence of synthetically lethal *alix-1 vps29-3*$^{(-/-)}$ mutants in the latter samples.

To test whether ALIX and retromer proteins also cooperate to transport soluble vacuolar proteins in vegetative tissues, we examined the trafficking of the fluorescently labeled soluble vacuolar marker aleurain-mRFP, which contains a sequence-specific vacuolar sorting signal with the canonical Asn-Pro-Ile-Arg (NPIR) motif (37). When transiently expressed in cotyledon epidermal cells of WT plants, the fluorescent vacuolar marker uniformly labeled the cell interior, occupied almost

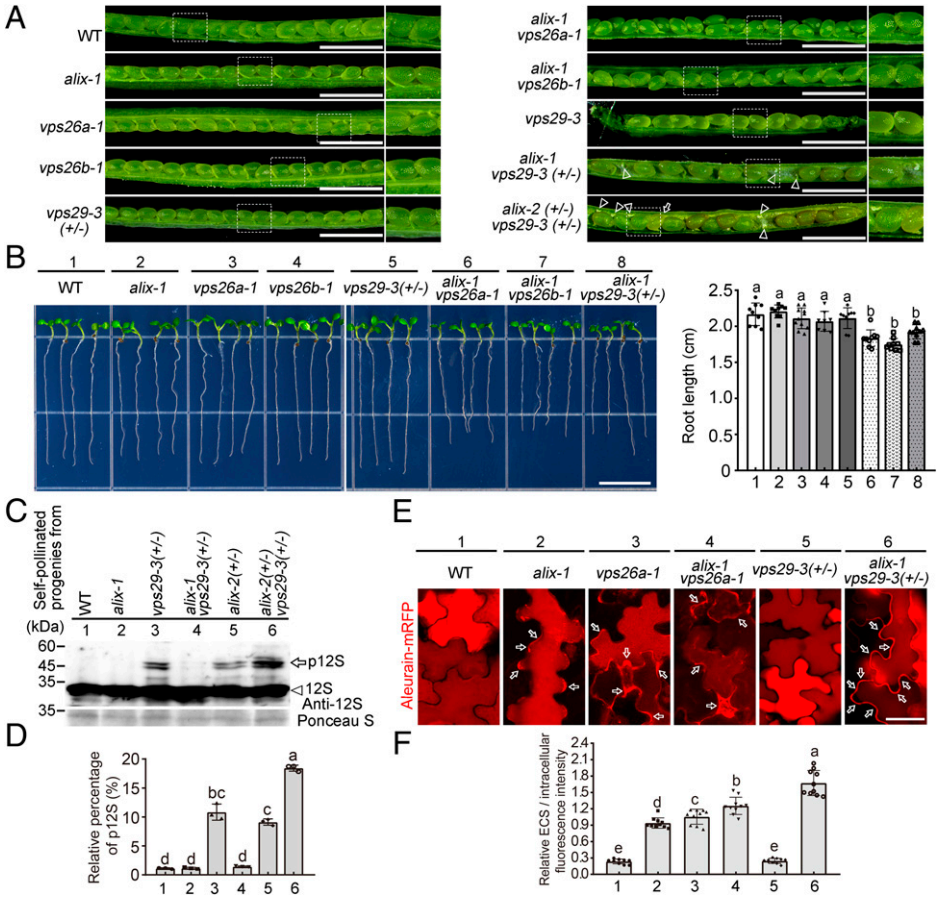

Fig. 4. ALIX shows genetic interaction with Vps26 or Vps29. (*A*) Phenotypes of progenies from 8-wk-old plant of indicated genotypes. The paler seeds from *alix-2*$^{(+/-)}$ *vps29-3*$^{(+/-)}$ mutant plant siliques (arrow) are *alix-2*$^{(-/-)}$ *vps29-3*$^{(+/-)}$. Note the slowed embryogenesis in siliques from *alix-2*$^{(+/-)}$ *vps29-3*$^{(+/-)}$ and *alix-1 vps29-3*$^{(+/-)}$ mutant plants (arrowheads). Scale bars, 1.5 mm. (*B*) Seven-day-old seedlings of indicated genotypes were photographed. The root length of seedlings of the indicated genotypes was quantified on the right. The numbers from 1 to 8 represent WT, *alix-1*, *vps26a-1*, *vps26b-1*, *vps29-3*$^{(+/-)}$, *alix-1 vps26a-1*, *alix-1 vps26b-1*, and *alix-1 vps29-3*$^{(+/-)}$, respectively. Error bars are the SD of nine seedlings from three independent experiments. Letters above bars indicate whether there are significant differences at $P = 0.05$ level. Scale bar, 1 cm. (*C*) Total protein extracts from seeds of self-pollinated progenies from indicated genotypes were analyzed by immunoblot analysis using anti-12S globulin antibody. Note seeds of progenies from *alix-2*$^{(+/-)}$ *vps29-3*$^{(+/-)}$ present higher accumulation of precursors of 12S globulin (p12S, arrow) than other genotypes. Arrowhead indicates mature 12S globulin (12S). (*D*) Quantification analysis of the p12S accumulation in seeds of progenies from indicated genotypes. The immunoblot intensity was normalized by the loading control of Ponceau S staining. The percentage of p12S in the total number of 12S proteins (p12S plus mature 12S globulin) was quantified. Error bars are the SD from three independent experiments. (*E*) Confocal images of cotyledon cells from *Arabidopsis* seedlings of the indicated genotypes transiently transformed with aleurain-mRFP. Note that in the *alix-1 vps26a-1* and *alix-1 vps29-3*$^{(+/-)}$ double mutants, aleurain-mRFP showed reduced fluorescent signal in LVs coupled to much stronger signal in the ECS (arrows), compared to that in WT or single mutants. Scale bar, 30 μm. (*F*) Relative extracellular to intracellular fluorescence intensity values. The region of interest (ROI) was kept constant for each measurement. Error bars are the SD of 10 cells from three independent experiments. Letters above bars indicate whether there are significant differences at $P = 0.05$ level.

entirely by the vacuole (Fig. 4*E*). In contrast, we observed partial secretion of the vacuolar marker, with RFP labeling the ECS, in *alix-1* and *vps26a-1* homozygous mutants, but not in *vps29-3*$^{(+/-)}$. Interestingly, in the *alix-1 vps26a-1* and *alix-1 vps29-3*$^{(+/-)}$ double mutants, aleurain-mRFP showed reduced vacuolar levels coupled to higher ($P < 0.01$) amounts of secretion into the ECS than in WT or single mutants (Fig. 4*F*), thus suggesting that the double mutants of *alix-1 vps26a-1* and *alix-1 vps29-3*$^{(+/-)}$ had much more severe defects in protein trafficking to the LV in vegetative tissues. Taken together with the evidence for direct physical interaction, these genetic interaction tests support the notion that ALIX, Vps26, and Vps29 function together in trafficking to both PSVs and LVs, an essential process for plant development and viability.

ALIX Is Required for Membrane Recruitment of Vps26 and Vps29 on MVB/PVC. If ALIX is incorporated into the retromer core complex, loss of ALIX function could affect retromer subunits. To test this hypothesis, we first compared the distribution of Vps26A-GFP or Vps29-GFP in cytosol and endosome in the root epidermal cells of WT and *ALIX-RNAi* plants. Interestingly, the intensity of fluorescence signal of Vps26A-GFP or Vps29-GFP decreased in the root epidermal cells of *DEX::ALIX-RNAi* plants after DEX induction (Fig. 5*A*, *Left* and *Middle*). However, the intensity of the fluorescence signal of YFP-RabG3f, an *Arabidopsis* Rab7 homolog participating in the recruitment of the core retromer to endosomes (35), was not affected in *ALIX-RNAi* plants (Fig. 5*A*, *Right*). In addition, the reduced fluorescence in Vps26A or Vps29 was not due to a decrease at transcript level in the *ALIX-RNAi* mutant (*SI Appendix*, Fig. S7*A*). Compared to the WT cells, the numbers of both Vps26A-GFP and Vps29-GFP punctae were also decreased in the root epidermal cells of *ALIX-RNAi* seedlings and the embryo cells of *alix-2* (Fig. 5*B* and *SI Appendix*, Fig. S7 *B* and *C*). This disturbance in Vps26-GFP or Vps29-GFP membrane recruitment in the DEX-treated *ALIX-RNAi* plants was confirmed by immunoblot analysis of membrane and soluble cellular fractions. Compared to the WT, an increased amount of Vps26 or Vps29 was found to distribute in the cell-soluble (CS) fraction with less in the cell membrane (CM)

fraction in *ALIX-RNAi* plants after DEX induction (Fig. 5 *C* and *D*). Interestingly, we also found a decrease in both endogenous Vps26A and Vps29-GFP protein levels in total protein extracts from *ALIX-RNAi* as compared to those in WT (Fig. 5*E*), suggesting that a deficiency of ALIX protein reduces the stability of both Vps26 and Vps29 proteins in the cytosol. Altogether, these results confirm that ALIX, Vps26, and Vps29 proteins function cooperatively in plant cells and that the assembly of the core retromer complex is disturbed in the *alix* mutant cells.

To refine this analysis, we analyzed the subcellular distribution of Vps26A-GFP and Vps29-GFP punctae relative to organelle markers in *DEX::ALIX-RNAi* mutant and WT plants (Fig. 5 *F* and *G* and *SI Appendix*, Fig. S7 *D*–*G*). The colocalization frequency of Vps26A-GFP and Vps29-GFP with MVB/PVC and TGN markers, but not with Golgi marker, was significantly decreased in *ALIX-RNAi* seedlings compared to WT plants (Fig. 5*H* and *SI Appendix*, Fig. S7 *D*–*G*). Moreover, Vps26A-GFP and Vps29-GFP presented reduced sensitivity to Wort treatment, as shown by the low percentage of colocalization with mCherry-Rha1 on the enlarged MVB/PVCs (Fig. 5 *I*–*K*). Taken together, these results indicate that correct endomembrane localization of Vps26 and Vps29 requires intact function of ALIX in planta.

ALIX Depletion Causes Mis-sorting and Abnormal Accumulation of VSR. In the plant protein transport pathway to vacuole, the retromer complex is responsible for the recycling of VSRs, which sort soluble proteins to the vacuoles (38, 39). Given our findings that ALIX depletion affects recruitment of the retromer core complex to the MVB/PVC membrane, the trafficking of VSRs would probably be disturbed. This prompted us to explore whether dysfunction of ALIX causes mislocalization of VSRs. We thus generated *AtVSR1pro::GFP-gAtVSR1* transgenic lines in WT, *alix-2*, and *DEX::ALIX-RNAi* backgrounds to investigate GFP-AtVSR1 subcellular localization. In the embryo cells of WT, GFP-AtVSR1 showed a punctate localization (Fig. 6*A*, *Left*). On the contrary, in *alix-2*, GFP-AtVSR1 showed signals at PM and formed aggregated clusters of intracellular punctate dots (Fig. 6*A*, *Middle* and *Right*). Next, we investigated the endosomal distribution of VSR by exploring the colocalization of GFP-AtVSR1 with endosomal markers. Quantification on the distribution of GFP-AtVSR1 within different organelles demonstrated a significant ($P < 0.01$) decrease of colocalization with MVB/PVC marker mCherry-Rha1 and TGN marker VHA-a1-RFP, but less-significant changes with Golgi marker mCherry-SYP32 in *alix-2* embryos relative to WT (Fig. 6 *B* and *C*). The PM localization and mislocalization of intracellular punctate dots were also observed in 5-d-old seedlings of *DEX::ALIX-RNAi* in the presence of DEX (*SI Appendix*, Fig. S8), suggesting that the depletion of ALIX causes mislocalization of VSRs in roots.

In addition to the endosomal localizations, VSRs can be transported into the vacuole reflecting VSR turnover (38, 40). Indeed, when GFP-AtVSR1 plants were incubated with the endocytic tracker FM4-64 for several hours in darkness, which promotes the stabilization of fluorescent protein-tagged reporters in the lytic compartment (41), a vacuolar accumulation of GFP-AtVSR1 was observed in control WT plants (Fig. 6*D*, *Left*). However, dark treatment did not cause an obvious vacuolar accumulation of GFP-AtVSR1 in *ALIX-RNAi* plants (Fig. 6*D*, *Right*), suggesting that vacuolar VSR turnover is compromised in *alix* mutants. To further confirm this, we extracted total proteins from embryo of the self-fertilized *alix-2* and *alix-4* siliques as well as from 5-d-old seedlings from *ALIX-RNAi* and WT plants and analyzed the accumulation of VSRs by immunoblot with anti-VSR antibodies. Higher numbers of VSRs accumulated in both *alix* mutant embryos and seedlings (Fig. 6 *E* and *F*), consistent with a reduced turnover in the vacuole.

To further investigate the localization of VSR and the ultrastructure of aggregated clusters of GFP-AtVSR1in *alix* mutant, the embryos of WT and *alix-2* mutant were used to perform immunogold labeling with anti-VSR antibody. Positive labeling for the TGN was obtained in both WT and *alix-2* samples (Fig. 6*G*, *Left* and *Middle*). As in the confocal observation, the VSR-positive dense vesicles (DVs) of *alix-2* in HPF samples were seen to accumulate as large clusters adjacent to or occasionally at some distance from the Golgi stack. In some cases, DVs within these clusters appear to fuse with each other (Fig. 6*G*, *Right*). Thus, the confocal observation of aggregated clusters of intracellular punctate dots of GFP-AtVSR1 in *alix-2* mutant (Fig. 6*A*) are probably the VSR-positive clusters of DVs at the ultrastructural level. Moreover, clustered vesicles labeled by anti-2S albumin antibody were also found in *alix-2* mutant, indicating cargoes were missorted to apoplast via these abnormal aggregated DVs in *alix* mutants (*SI Appendix*, Fig. S9). Interestingly, we observed fusion of anti-VSR labeled electron-opaque vesicles with the PM in sections from *alix-2* samples (Fig. 6*H*). Such structures were not seen in WT samples. Moreover, a significantly higher number of gold particles were found at the PM in *alix-2* mutant ($10.9 \pm 4.4/\mu m^2$; $n = 9$) compared to that in WT ($1.6 \pm 1.7/\mu m^2$; $n = 10$). Taken together, these data support the idea that impaired recruitment of retromer and, consequently, mislocalization of VSRs leads to the secretion of vacuole proteins in *alix* mutants.

Discussion

Although previous reports have demonstrated that mutation of plant ESCRT proteins AMSH3 and FREE1 can lead to defects in sorting of soluble vacuolar proteins into LVs or PSVs (42, 43), the regulatory mechanism of underlying ESCRT involvement in this trafficking process remains unknown. To summarize our findings, we here identified a plant ESCRT-associated ALIX protein that regulates vacuolar trafficking of soluble proteins by demonstrating the following: 1) dysfunction of ALIX causes defects in transport of soluble vacuolar proteins, leading to their secretion into the ECS; 2) ALIX is incorporated into the retromer core subcomplex via the direct binding to Vps26 and Vps29; 3) ALIX and core retromer proteins interact genetically to mediate trafficking of soluble vacuolar proteins; and 4) depletion of ALIX disturbs the membrane association of Vps26 and Vps29 on endosome membrane, in turn leading to the mislocalization of VSRs and, thus, disturbing vacuolar protein trafficking. These observations would seem to argue that ALIX regulates the recruitment of retromer core subcomplex via binding to Vps26 and Vps29, which mediates retrograde transport of VSRs necessary for proper sorting of soluble vacuolar cargo.

The regulatory mechanism of ALIX presented here is distinct from the previously proposed hypothesis that ESCRT machinery may play potential functions in the fusion event between vesicles and lysosomes/vacuoles (42), which is supported by the finding in mammalian cells that ESCRT proteins can interact with homotypic fusion and vacuole protein sorting (HOPS) complex and that less Rab7 GTPase is recruited to the endosomal membrane in the ESCRT mutant than WT (44–46). In contrast, our studies suggest that the recruitment to the endosomal membrane of *Arabidopsis* Rab7 GTPase homolog RabG3f is not disturbed in the ALIX mutant (Fig. 5*A*). It could also be

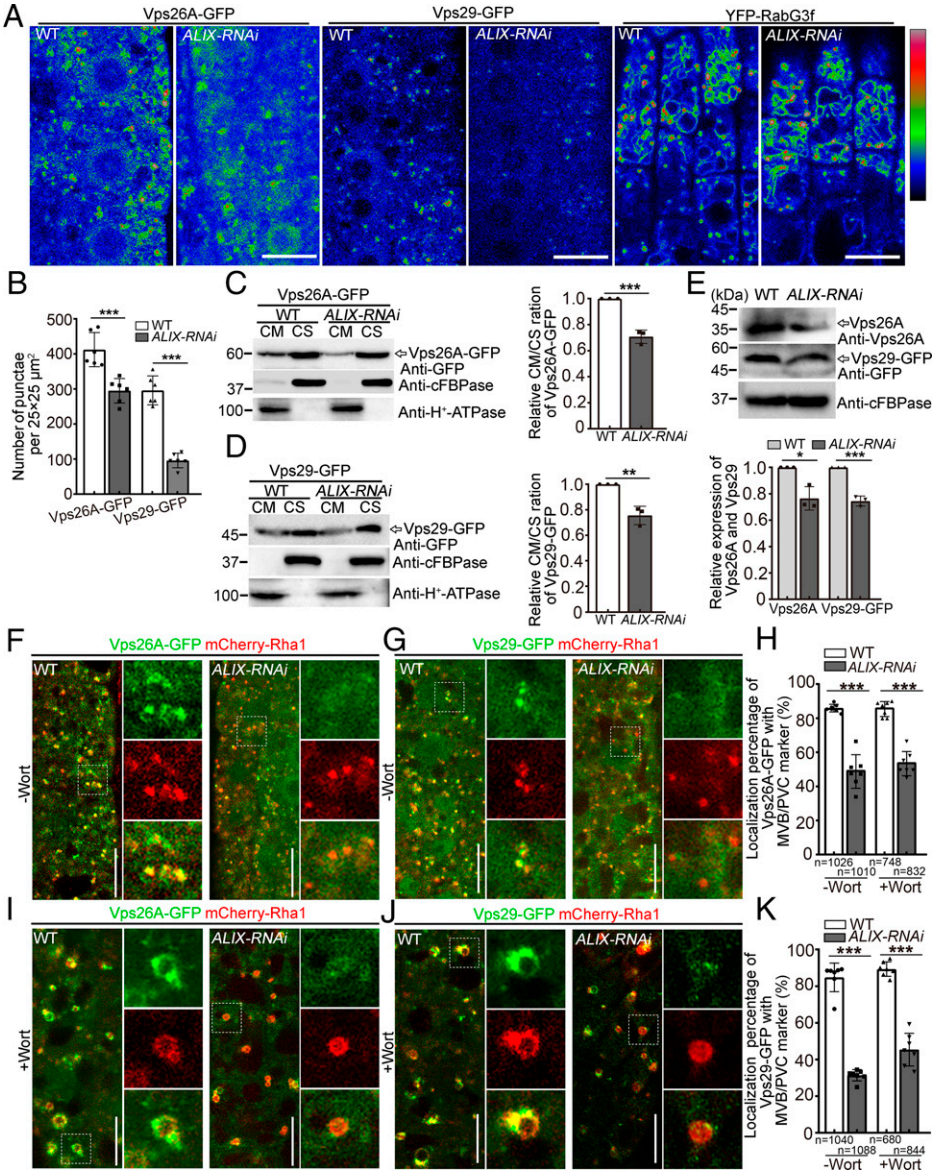

Fig. 5. ALIX regulates Vps26 and Vps29 recruitment to MVB/PVCs. (*A*) Fluorescence intensity of Vps26A-GFP (*Left*), Vps29-GFP (*Middle*), and YFP-RabG3f (*Right*) in the WT or *DEX::ALIX-RNAi* plant after DEX induction. False color code was used for intensity visualization. (*B*) Quantification (mean ± SD) of the number of Vps26A-GFP and Vps29-GFP punctuated structures per 25 × 25 μm^2 in WT and *DEX::ALIX-RNAi* after DEX treatment. ***$P < 0.001$ in Student's *t* test. (*C* and *D*) Immunoblot analysis of Vps26-GFP and Vps29-GFP membrane association in WT and *DEX::ALIX-RNAi* plants after DEX induction. The intensity of Vps26-GFP or Vps29-GFP was normalized by the loading control of anti-H$^+$-ATPase as CM fraction and anti-cFBPase as CS fraction, and the CM/CS ratio in indicated genotype seedlings is quantified on the right. Error bars are the SD from three independent experiments. **$P < 0.01$, ***$P < 0.001$ in Student's *t* test. (*E*) Immunoblot analysis of endogenous Vps26A and Vps29-GFP on total protein extracts from WT or *DEX::ALIX-RNAi* plant after DEX induction using anti-Vps26 and anti-GFP, respectively. Anti-cFBPase, a ubiquitously expressed cytosolic fructose-1,6-bisphosphatase, was used as loading control. Protein levels of Vps26A and Vps29-GFP were quantified on the bottom. *$P < 0.05$, ***$P < 0.001$ in Student's *t* test. (*F* and *G*) Localization of Vps26A-GFP (*F*) or Vps29-GFP (*G*) and mCherry-Rha1 in root epidermis cells of DEX-treated WT or *DEX::ALIX-RNAi* plant. Scale bar, 10 μm. (*H*) Number of mCherry-Rha1 compartments containing Vps26A-GFP (*Top*) or Vps29-GFP (*Bottom*) signals in WT or *DEX::ALIX-RNAi* plant after DEX induction without (−) or with (+) Wort treatment. n, total numbers of analyzed punctae. ***$P < 0.001$ in Student's *t* test. (*I* and *J*) Localization of Vps26A-GFP (*I*) or Vps29-GFP (*J*) and mCherry-Rha1 in root epidermis cells of DEX-treated WT or *DEX::ALIX-RNAi* plant with (+) Wort treatment. Note that neither Vps26A-GFP nor Vps29-GFP localizes on mCherry-Rha1-labeled Wort-enlarged MVB/PVCs. Scale bar, 10 μm.

argued that soluble vacuolar proteins mis-sorting in ALIX and ESCRT mutants could be an indirect effect of the abnormalities observed in MVB/PVCs and vacuole biogenesis in the mutant. However, such an argument is challenged by recent data showing that the depletion of the ESCRT regulator FYVE4, which alters the formation of ILVs in MVB/PVCs and vacuole biogenesis, shows a defect in degradative vacuolar sorting of membrane proteins but not of soluble vacuolar cargoes transported to LVs or PSVs (16). Although the possible interactions of ALIX with other trafficking regulators, like the HOPS complex, need future investigation, our data showing an interaction between ALIX and core retromer proteins now put the ESCRT machinery into a functional context within the soluble protein vacuolar pathway.

In the root cells of *Arabidopsis alix* mutants, smaller or empty MVB/PVCs without ILVs are occasionally observed forming clusters (21, 23). Without normally functioning MVB/PVCs in ESCRT mutant, numerous smaller vacuoles aggregated inside the cell and finally lead to abnormal LVs, thus suggesting the importance of ESCRT for LV biogenesis (47, 48). Interestingly, our ultrastructural analysis of embryos cells in *alix-2* mutant observed large clustered DVs, which was similar with

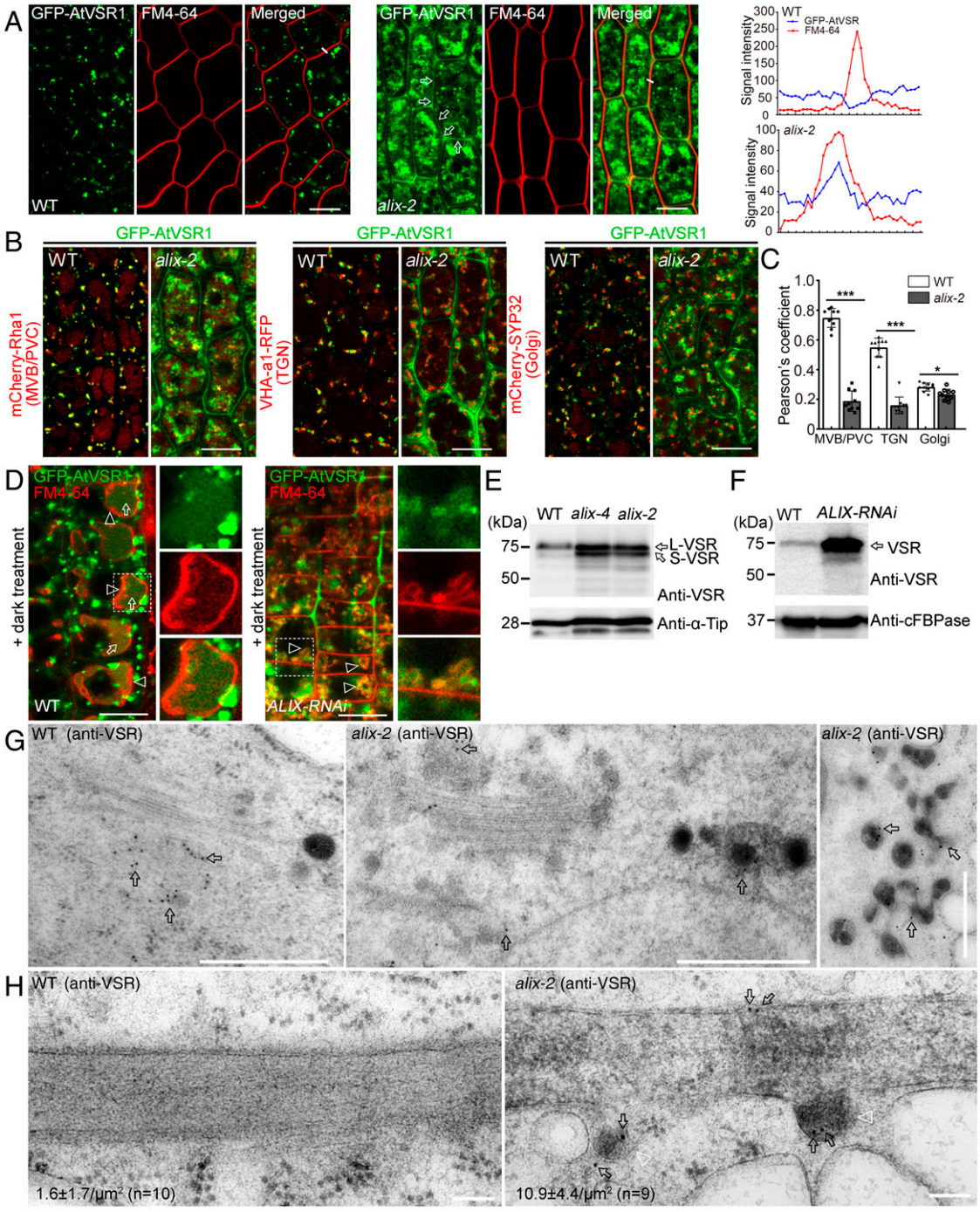

Fig. 6. ALIX depletion causes the mislocalization of VSR. (*A*) Localization of GFP-AtVSR1 in WT (*Left*) and *alix*-2 (*Middle*) mutant. Note the colocalization of GFP-AtVSR1 with PM staining dye FM4-64 in *alix-2* mutant. The embryos expressing GFP-AtVSR1 in the indicated genotypes were observed under confocal after staining with FM4-64 for 1 min. FM4-64 was used as a PM marker. ImageJ quantifications of green (blue lines) and red (red lines) signal intensities for indicated white lines are shown (*Right*). Scale bars, 10 μm. (*B*) Colocalization analysis of GFP-AtVSR1 with endosomal markers in embryo cells of WT or *alix-2* mutant. Colocalizations of GFP-AtVSR1 with the MVB/PVC marker mCherry-Rha1 (*Left*), TGN marker VHA-a1-RFP (*Middle*), and the Golgi marker mCherry-SYP32 (*Right*) were analyzed with a confocal microscope. Scale bars, 10 μm. (*C*) Pearson colocalization coefficients of GFP-AtVSR1 with MVB/PVC marker mCherry-Rha1, TGN marker VHA-a1-RFP, and the Golgi marker mCherry-SYP32 in WT and *alix-2* plants. The results were obtained from 10 individual seedlings. Error bars are the SD. $*P < 0.05$, $***P < 0.001$ in Student's *t* test. (*D*) ALIX depletion alters GFP-AtVSR1 vacuolar trafficking. Seven-day-old seedlings of indicated genotypes with DEX induction were incubated with FM4-64 and visualized after 6 h dark treatment. Arrows and arrowheads indicate the vacuolar GFP signal and tonoplast-localized RFP signal, respectively. Separated images of each channel in the white outline area are shown on the right side (from top to bottom: GFP, RFP, and merged). Scale bars, 10 μm. (*E*) Immunoblot analysis of protein from embryo cells of *Arabidopsis* WT or *alix-2* or *alix-4* mutants. Anti-VSR was used to detect endogenous VSR. Anti-α-Tip, a tonoplast intrinsic protein, is used as a loading control. The VSR produced two bands: L-VSR and S-VSR. (*F*) Immunoblot analysis of protein from 7-d-old seedlings of indicated genotypes with DEX induction. Anti-VSR was used to detect endogenous VSR. The cytoplasmic marker anti-cFBPase is used as a loading control. (*G*) Immunoelectron micrograph of WT and *alix-2* embryo cells with anti-VSR antibody. Note the accumulation of large clusters of VSR-labeled DVs in *alix-2* cells (*Right*). Ultrathin sections were prepared from HPF/FS samples of indicated genotype embryo cells, followed by immunogold labeling using VSR antibody. Arrows indicate the gold particles. Scale bars, 500 nm. (*H*) Ultrastructural analysis of the fusion profiles between VSR-labeled DVs and PM in developing embryo cells of *alix-2* mutant. Ultrathin sections were prepared from HPF/FS samples of indicated genotype embryo cells, followed by immunogold labeling using VSR antibodies. Arrows and arrowheads indicate the gold particles and DVs, respectively. The number of anti-VSR gold particles per field along the PM is quantified in the bottom. The results were obtained from 10 individual IEM images. Error bars are the SD. Scale bars, 100 nm.

the MVB/PVC cluster in root cells. It is possible that the accumulation of large clustered DVs may be related to the defect of PSV biogenesis in embryo cells of *alix* mutants. Due to the resolution differences between confocal and electron microscopy, the sizes of vesicle clusters observed are slightly different. It will be interesting to apply correlative light and electron microscopy and whole-cell 3D electron tomography at nanometer-level resolutions to further explore the nature and membrane source of these large clustered DVs. In addition, future research should identify ALIX interaction factors that may control the integrity of LV/PSV, which will certainly shed light on the biological significance of ESCRT in vacuole biogenesis in plants.

Depletion of ALIX Leads to the Cosecretion of VSRs and Cargo Proteins. The VSRs act in sorting soluble cargo to the LVs in vegetative cells or storage proteins to the PSVs during seed development. Consistent with previous results, in addition to the MVB/PVCs and TGN localizations, VSRs were found in the vacuolar lumen (Fig. 6*D*), presumably for their turnover (38, 40). In yeast cells, retromer mutants exhibit increased degradation of Vps10p in the vacuole (49). Similarly, in *Arabidopsis* Vps29 mutants, a substantial amount of VSR was transported to the LV, rather than being recycled from the MVB/PVC to the TGN (38). Unexpectedly, and not previously reported for the ALIX mutant, a large proportion of endogenous VSRs accumulated in the endosomes and were also found to locate to the PM by confocal microscopy of functional fluorescence-tagged VSR and immuno-electron microscopy (IEM) with VSR antibodies (Fig. 6 *A* and *H*). PM-localized VSR proteins have been found in germinating pollen tubes and were assumed to reflect that in pollen tubes, VSRs are diverted into secretory vesicles and reach the PM for delivery of soluble cargo proteins to the apoplast (50). The large accumulations of clustered DVs, together with the observation of VSR-labeled electron-opaque vesicles fusing with the PM in the embryo cells of *alix* mutant, indicate a rerouting of vacuolar proteins and their receptors in the absence of ALIX activity. The presence of vesicle clusters containing storage protein precursors and VSRs fusing with the PM can also been observed in *nhx5 nhx6* embryo cells or Wortmannin-treated mung bean cotyledon (51, 52), which is probably due to the dysfunction of VSRs causing the redirection of vacuolar proteins into the bulk flow secretion pathway (53). Here, we have suggested that the inhibitory effect on the transport of vacuolar proteins into the LVs/PSVs in the *alix* mutant is linked to defects in retromer-mediated recycling of VSRs.

The retromer is a key protein complex involved in VSR recycling and retrograde transport in plants (36, 38, 54), so determining the subcellular localization of the retromer complex could be assumed to reveal the compartment from where VSRs retrieve. However, the subcellular localization of the retromer complex in plants is still controversial (11, 32). In our studies, functional fluorescently tagged Vps26 and Vps29 proteins were mainly colocalized with MVB/PVC markers and partially with the TGN marker, but not with the Golgi markers in both *Arabidopsis* embryo cells and root meristem cells, which is inconsistent with previous reports of Vps29 and Vps35 proteins in *Arabidopsis* root meristem cells (29, 54). In contrast, fluorescence immunolocalization-based colocalization analysis in *Arabidopsis* roots or tobacco BY2 cells revealed that endogenous Vps29 localized at the TGN along with SNXs (55). To address these issues and attempt to consolidate these data, it has been proposed that the *Arabidopsis* retromer may function both in protein sorting at the TGN and during the early stages of MVB formation (31, 56). Further experiments, such as the *in situ* interaction analysis (57) and intracellular pH measurements (52, 58, 59), will be essential to unequivocally stablish where VSRs release their cargoes and which compartments are involved in their recycling route.

ALIX May Function to Stabilize the Retromer Core Subcomplex. Assembly and association of the core retromer proteins onto the endosome membranes appear to be different in plants than in yeast and mammalian cells. In plants, it has been proposed that the core retromer Vps26-Vps29-Vps35 assembles in the cytosol and is then recruited to the endosomal membrane, independently of SNX proteins, through binding of Vps35 to activated RABG3f (35). However, interactions of Vps26 and Vps29 with Vps35 alone are probably not enough for proper retromer recruitment and function, as emerging evidence demonstrates that the deletion of Vps26 strongly affects the membrane association of Vps29, while a direct interaction between Vps26 and Vps29 has never been established (29). Indeed, the work presented here provides evidence that in plants, ALIX forms a complex with Vps26 and Vps29 and regulates their membrane associations onto the MVB/PVCs, suggesting that ALIX may function to stabilize the interaction of Vps26 and Vps29 with Vps35. Our studies suggest that the ALIX Bro1 domain is responsible for interaction with Vps26 and Vps29 (Fig. 2*F*). It is possible that the ALIX forms dimers (22, 60) to enable the interaction of Bro1D with Vps26 and Vps29. In conclusion, it appears that the plant ALIX may have evolved a unique mechanism that can stabilize the retromer core subcomplex to enable it to function.

Based on the findings of this study and the previous literature in plants, we propose the following working model of ALIX function in plants (*SI Appendix*, Fig. S10): 1) ALIX mainly localizes in the cytosol and can be recruited into membrane compartments by SNF7 or Vps23 as canonical ESCRT proteins for sorting ubiquitinated membrane proteins into vacuole and regulating MVB/PVCs biogenesis; 2) ALIX forms homodimers and binds to Vps26 and Vps29 through the Bro1D to stabilize the retromer core subcomplex. The core retromer assembles in the cytosol with Vps35 directly binding to Vps26 and Vps29. Then, the subcomplex is recruited to membrane through Vps35 via the interaction with the Rab7 homolog RABG3f; 3) Vps35 interacts with the C terminus of VSRs. Hence, ALIX coordinates with core retromer proteins participating in the recycling of VSRs for soluble vacuolar protein sorting; and 4) depletion of ALIX leads to the failure of retromer core complex recruitment, thereby causing the mislocalization and secretion of VSRs together with soluble vacuolar proteins. The nature of the compartment that secretes VSRs and their cargoes, as well as the vesicles that fuse with the PM in *alix* mutants, and the machinery regulating this fusion event are topics for future research.

It will be important to identify other components of ESCRT machinery that are required to regulate retromer trafficking. In addition, it will be interesting to identify factors or environmental cues that may regulate the balance between the recruitment of ALIX into ESCRT complex for degradation of membrane proteins vacuolar or into the retromer subcomplex for recycling VSRs and enabling vacuolar protein sorting.

Materials and Methods

Additional materials and methods, including plasmid construction, plant materials, plant growth and chemical treatments, transient expression in *Arabidopsis*, immunofluorescence labeling in *Arabidopsis* roots, confocal microscopy and FRET analysis, Y2H analysis, protein preparation, IP and immunoblotting, recombinant protein purification and *in vitro* binding assay, TEM study, antibodies, RNA extraction and RT-PCR analysis,

quantification and statistical analysis, and accession numbers are described in *SI Appendix*.

Data Availability. All study data are included in the article and/or *SI Appendix*. This article does not contain datasets, code, or materials in addition to those included.

ACKNOWLEDGMENTS. We thank Lorenzo Frigerio (University of Warwick) for sharing transgenic plants expressing spL-RFP, Vicente Rubio (Centro Nacional de Biotecnología) for providing with *alix-1* mutant and transgenic plant expressing GFP-ALIX, and Nam-Hai Chua (The Rockefeller University) for the binary vector pTA7002. This work was supported by grants from the National Natural Science Foundation of China (31970181 and 32170342), the Zhejiang Provincial Natural Science Foundation of China (LR20C020001), the Fundamental Research Funds for the Provincial Universities of Zhejiang (2020KJ001), the Research Grants Council of Hong Kong (R4005-18), the Zhejiang A&F University Starting Funding (2018FR029), and the 111 Project (D18008) to J.S; the China Postdoctoral Science Foundation (2020M681919) to S.H.; the NSFC grant (31670179 and 91854201) and Research Grants Council of Hong Kong (AoE/M-05/12, C4012-16E, C4033-19E, and C4002-17G) to L.J.; grant PGC2018-094257-B-C21 MCIN/AEI/10.13039/501100011033/FEDER "una manera de hacer Europa" to E.R.; Grants-in-Aid for Scientific Research from the Japan Society for the Promotion of Science (15H05776) and the Hirao Taro Foundation of KONAN GAKUEN for Academic Research to I.H.-N; and the National Natural Science Foundation of China (31870171, 32061160467) and Fok Ying-Tong Education Foundation for Young Teachers (171014) to C.G.

Author affiliations: [a]State Key Laboratory of Subtropical Silviculture, Zhejiang A&F University, 311300 Hangzhou, China; [b]Centre for Cell & Developmental Biology and State Key Laboratory of Agrobiotechnology, School of Life Sciences, The Chinese University of Hong Kong, Shatin, New Territories, Hong Kong, China; [c]Central European Institute of Technology, Mendel University in Brno, CZ-61300 Brno, Czech Republic; [d]Centro Nacional de Biotecnología, Consejo Superior de Investigaciones Cientificas, Cantoblanco, E-28049 Madrid, Spain; [e]Guangdong Provincial Key Laboratory of Biotechnology for Plant Development, School of Life Sciences, South China Normal University, Guangzhou, 510631, China; [f]Graduate School of Science, Kyoto University, Sakyo-ku, Kyoto 606-8502, Japan; [g]Faculty of Science and Engineering, Konan University, Kobe 658-8501, Japan; and [h]The Chinese University of Hong Kong Shenzhen Research Institute, Shenzhen, 518057 China

1. G. Jürgens, Membrane trafficking in plants. *Annu. Rev. Cell Dev. Biol.* **20**, 481–504 (2004).
2. X. Wang *et al.*, The roles of endomembrane trafficking in plant abiotic stress responses. *J. Integr. Plant Biol.* **62**, 55–69 (2020).
3. L. Frigerio, G. Hinz, D. G. Robinson, Multiple vacuoles in plant cells: Rule or exception? *Traffic* **9**, 1564–1570 (2008).
4. T. Shimada *et al.*, Vacuolar sorting receptor for seed storage proteins in *Arabidopsis thaliana*. *Proc. Natl. Acad. Sci. U.S.A.* **100**, 16095–16100 (2003).
5. K. Fuji *et al.*, Arabidopsis vacuolar sorting mutants (green fluorescent seed) can be identified efficiently by secretion of vacuole-targeted green fluorescent protein in their seeds. *Plant Cell* **19**, 597–609 (2007).
6. J. Zouhar, A. Muñoz, E. Rojo, Functional specialization within the vacuolar sorting receptor family: VSR1, VSR3 and VSR4 sort vacuolar storage cargo in seeds and vegetative tissues. *Plant J.* **64**, 577–588 (2010).
7. D. Zhu, M. Zhang, C. Gao, J. Shen, Protein trafficking in plant cells: Tools and markers. *Sci. China Life Sci.* **63**, 343–363 (2020).
8. J. Shen *et al.*, An in vivo expression system for the identification of cargo proteins of vacuolar sorting receptors in Arabidopsis culture cells. *Plant J.* **75**, 1003–1017 (2013).
9. E. Watanabe, T. Shimada, M. Kuroyanagi, M. Nishimura, I. Hara-Nishimura, Calcium-mediated association of a putative vacuolar sorting receptor PV72 with a propeptide of 2S albumin. *J. Biol. Chem.* **277**, 8708–8715 (2002).
10. G. P. Di Sansebastiano, F. Barozzi, G. Piro, J. Denecke, C. de Marcos Lousa, Trafficking routes to the plant vacuole: Connecting alternative and classical pathways. *J. Exp. Bot.* **69**, 79–90 (2017).
11. D. G. Robinson, Retromer and VSR recycling: A red herring? *Plant Physiol.* **176**, 483–484 (2018).
12. J. A. MacGurn, P. C. Hsu, S. D. Emr, Ubiquitin and membrane protein turnover: From cradle to grave. *Annu. Rev. Biochem.* **81**, 231–259 (2012).
13. L. G. Richardson *et al.*, Protein-protein interaction network and subcellular localization of the *Arabidopsis thaliana* ESCRT machinery. *Front Plant Sci* **2**, 20 (2011).
14. V. Winter, M.-T. Hauser, Exploring the ESCRTing machinery in eukaryotes. *Trends Plant Sci.* **11**, 115–123 (2006).
15. F. C. Reyes *et al.*, A novel endosomal sorting complex required for transport (ESCRT) component in *Arabidopsis thaliana* controls cell expansion and development. *J. Biol. Chem.* **289**, 4980–4988 (2014).
16. C. Liu *et al.*, A plant-unique ESCRT component, FYVE4, regulates multivesicular endosome biogenesis and plant growth. *New Phytol.* **231**, 193–209 (2021).
17. C. Gao *et al.*, A unique plant ESCRT component, FREE1, regulates multivesicular body protein sorting and plant growth. *Curr. Biol.* **24**, 2556–2563 (2014).
18. C. Kolb *et al.*, FYVE1 is essential for vacuole biogenesis and intracellular trafficking in Arabidopsis. *Plant Physiol.* **167**, 1361–1373 (2015).
19. Q. Zhao *et al.*, RST1 is a FREE1 suppressor that negatively regulates vacuolar trafficking in Arabidopsis. *Plant Cell* **31**, 2152–2168 (2019).
20. J. Shen *et al.*, A plant Bro1 domain protein BRAF regulates multivesicular body biogenesis and membrane protein homeostasis. *Nat. Commun.* **9**, 3784 (2018).
21. K. Kalinowska *et al.*, Arabidopsis ALIX is required for the endosomal localization of the deubiquitinating enzyme AMSH3. *Proc. Natl. Acad. Sci. U.S.A.* **112**, E5543–E5551 (2015).
22. X. Cardona-López *et al.*, ESCRT-III-Associated Protein ALIX mediates high-affinity phosphate transporter trafficking to maintain phosphate homeostasis in Arabidopsis. *Plant Cell* **27**, 2560–2581 (2015).
23. J. Shen *et al.*, AtBRO1 functions in ESCRT-I complex to regulate multivesicular body protein sorting. *Mol. Plant* **9**, 760–763 (2016).
24. M. García-León *et al.*, Arabidopsis ALIX regulates stomatal aperture and turnover of abscisic acid receptors. *Plant Cell* **31**, 2411–2429 (2019).
25. P. R. Hunter, C. P. Craddock, S. Di Benedetto, L. M. Roberts, L. Frigerio, Fluorescent reporter proteins for the tonoplast and the vacuolar lumen identify a single vacuolar compartment in Arabidopsis cells. *Plant Physiol.* **145**, 1371–1382 (2007).
26. E. Rojo, V. K. Sharma, V. Kovaleva, N. V. Raikhel, J. C. Fletcher, CLV3 is localized to the extracellular space, where it activates the Arabidopsis CLAVATA stem cell signaling pathway. *Plant Cell* **14**, 969–977 (2002).
27. M. Sanmartín *et al.*, Divergent functions of VTI12 and VTI11 in trafficking to storage and lytic vacuoles in Arabidopsis. *Proc. Natl. Acad. Sci. U.S.A.* **104**, 3645–3650 (2007).
28. M. O. Delgadillo *et al.*, MTV proteins unveil ER- and microtubule-associated compartments in the plant vacuolar trafficking pathway. *Proc. Natl. Acad. Sci. U.S.A.* **117**, 9884–9895 (2020).
29. Y. Jaillais *et al.*, The retromer protein VPS29 links cell polarity and organ initiation in plants. *Cell* **130**, 1057–1070 (2007).
30. Y. Jaillais, I. Fobis-Loisy, C. Miège, C. Rollin, T. Gaude, AtSNX1 defines an endosome for auxin-carrier trafficking in Arabidopsis. *Nature* **443**, 106–109 (2006).
31. N. Heucken, R. Ivanov, The retromer, sorting nexins and the plant endomembrane protein trafficking. *J. Cell Sci.* **131**, jcs203695 (2018).
32. D. G. Robinson, J. M. Neuhaus, Receptor-mediated sorting of soluble vacuolar proteins: Myths, facts, and a new model. *J. Exp. Bot.* **67**, 4435–4449 (2016).
33. S. G. Jha *et al.*, Vacuolar Protein Sorting 26C encodes an evolutionarily conserved large retromer subunit in eukaryotes that is important for root hair growth in *Arabidopsis thaliana*. *Plant J.* **94**, 595–611 (2018).
34. J. Wang, Y. Cai, Y. Miao, S. K. Lam, L. Jiang, Wortmannin induces homotypic fusion of plant prevacuolar compartments. *J. Exp. Bot.* **60**, 3075–3083 (2009).
35. E. Zelazny *et al.*, Mechanisms governing the endosomal membrane recruitment of the core retromer in Arabidopsis. *J. Biol. Chem.* **288**, 8815–8825 (2013).
36. T. Shimada *et al.*, AtVPS29, a putative component of a retromer complex, is required for the efficient sorting of seed storage proteins. *Plant Cell Physiol.* **47**, 1187–1194 (2006).
37. D. Humair, D. Hernández Felipe, J. M. Neuhaus, N. Paris, Demonstration in yeast of the function of BP-80, a putative plant vacuolar sorting receptor. *Plant Cell* **13**, 781–792 (2001).
38. H. Kang *et al.*, Trafficking of vacuolar proteins: The crucial role of Arabidopsis vacuolar protein sorting 29 in recycling vacuolar sorting receptor. *Plant Cell* **24**, 5058–5073 (2012).
39. S. Hu, Y. Li, J. Shen, A diverse membrane interaction network for plant multivesicular bodies: Roles in proteins vacuolar delivery and unconventional secretion. *Front Plant Sci* **11**, 425 (2020).
40. H. Wang *et al.*, Vacuolar sorting receptors (VSRs) and secretory carrier membrane proteins (SCAMPs) are essential for pollen tube growth. *Plant J.* **61**, 826–838 (2010).
41. K. Tamura *et al.*, Why green fluorescent fusion proteins have not been observed in the vacuoles of higher plants. *Plant J.* **35**, 545–555 (2003).
42. C. Gao *et al.*, Dual roles of an Arabidopsis ESCRT component FREE1 in regulating vacuolar protein transport and autophagic degradation. *Proc. Natl. Acad. Sci. U.S.A.* **112**, 1886–1891 (2015).
43. E. Isono *et al.*, The deubiquitinating enzyme AMSH3 is required for intracellular trafficking and vacuole biogenesis in *Arabidopsis thaliana*. *Plant Cell* **22**, 1826–1837 (2010).
44. D. Metcalf, A. M. Isaacs, The role of ESCRT proteins in fusion events involving lysosomes, endosomes and autophagosomes. *Biochem. Soc. Trans.* **38**, 1469–1473 (2010).
45. H. Urwin *et al.*; FReJA Consortium, Disruption of endocytic trafficking in frontotemporal dementia with CHMP2B mutations. *Hum. Mol. Genet.* **19**, 2228–2238 (2010).
46. P. R. Pryor, J. P. Luzio, Delivery of endocytosed membrane proteins to the lysosome. *Biochim. Biophys. Acta* **1793**, 615–624 (2009).
47. Y. Cui, Q. Zhao, S. Hu, L. Jiang, Vacuole biogenesis in plants: How many vacuoles, how many models? *Trends Plant Sci.* **25**, 538–548 (2020).
48. Y. Cui *et al.*, A whole-cell electron tomography model of vacuole biogenesis in Arabidopsis root cells. *Nat. Plants* **5**, 95–105 (2019).
49. M. N. Seaman, E. G. Marcusson, J. L. Cereghino, S. D. Emr, Endosome to Golgi retrieval of the vacuolar protein sorting receptor, Vps10p, requires the function of the VPS29, VPS30, and VPS35 gene products. *J. Cell Biol.* **137**, 79–92 (1997).
50. H. Wang, X. H. Zhuang, S. Hillmer, D. G. Robinson, L. W. Jiang, Vacuolar sorting receptor (VSR) proteins reach the plasma membrane in germinating pollen tubes. *Mol. Plant* **4**, 845–853 (2011).
51. J. Wang, Y. C. Tse, G. Hinz, D. G. Robinson, L. Jiang, Storage globulins pass through the Golgi apparatus and multivesicular bodies in the absence of dense vesicle formation during early stages of cotyledon development in mung bean. *J. Exp. Bot.* **63**, 1367–1380 (2012).
52. M. Reguera *et al.*, pH regulation by NHX-type antiporters is required for receptor-mediated protein trafficking to the vacuole in Arabidopsis. *Plant Cell* **27**, 1200–1217 (2015).
53. L. L. P. daSilva *et al.*, Receptor salvage from the prevacuolar compartment is essential for efficient vacuolar protein targeting. *Plant Cell* **17**, 132–148 (2005).
54. M. Yamazaki *et al.*, Arabidopsis VPS35, a retromer component, is required for vacuolar protein sorting and involved in plant growth and leaf senescence. *Plant Cell Physiol.* **49**, 142–156 (2008).
55. S. Niemes *et al.*, Retromer recycles vacuolar sorting receptors from the *trans*-Golgi network. *Plant J.* **61**, 107–121 (2010).
56. D. Scheuring *et al.*, Multivesicular bodies mature from the *trans*-Golgi network/early endosome in Arabidopsis. *Plant Cell* **23**, 3463–3481 (2011).
57. S. Früholz, F. Fäßler, Ü. Kolukisaoglu, P. Pimpl, Nanobody-triggered lockdown of VSRs reveals ligand reloading in the Golgi. *Nat. Commun.* **9**, 643 (2018).
58. A. Martinière *et al.*, In vivo intracellular pH measurements in tobacco and Arabidopsis reveal an unexpected pH gradient in the endomembrane system. *Plant Cell* **25**, 4028–4043 (2013).
59. J. Shen *et al.*, Organelle pH in the Arabidopsis endomembrane system. *Mol. Plant* **6**, 1419–1437 (2013).
60. R. Pires *et al.*, A crescent-shaped ALIX dimer targets ESCRT-III CHMP4 filaments. *Structure* **17**, 843–856 (2009).